

**Morphometric Measurements of
Martian Valley Networks from
Mars Orbiter Laser Altimeter (MOLA) Data**

Rebecca M. E. Williams¹ and Roger J. Phillips
McDonnell Center for the Space Sciences and
Department of Earth and Planetary Sciences, Washington University, St. Louis, MO 63130

¹Now at Malin Space Science Systems, Inc., San Diego, CA 92191

Submitted to *Journal of Geophysical Research*
October 2000
Accepted January 2001

Abstract

Morphometric measurements of martian valley networks using Mars Orbiter Laser Altimeter (MOLA) topographic data yield mean valley width values of $\bar{x} \pm \sigma : 2040 \pm 1548$ m and depth values of $\bar{x} \pm \sigma : 109 \pm 137$ m. Our analysis of changes in valley shape with latitude and wall slope with depth indicate infilling and mass wasting processes have not greatly altered the original valley shape; thus, valley network morphometry is dominantly due to channel formation mechanisms. Both U- and V-shape profiles are observed, commonly within the same valley network system. The average U-shape valley is slightly deeper (18 m) and significantly wider (1313 m) than its V-shape counterpart. Valley networks have decreasing width-to-depth ratios and increasing wall slopes as valley depth increases. Our observations are consistent with a two-phase valley network formation model proposed by *Baker and Partridge* [1986]. (1) Valleys initially form via surface runoff, a process that creates V-shape profiles and quasi-dendritic form. The observed linear correlation of top width and depth (below 125 m depth) suggests the depth of vertical incisement governs top width. (2) Reactivation of the same valleys by headward extending sapping processes widens the channel to form U-shape cross-sections in downstream reaches. The availability of liquid water within a few hundred meters of the surface appears to be a necessary requirement for valley network formation. Mean valley depth decreases by ~50 m from equatorial to higher latitudes (~50°), contrary to the relationship predicted if the sapping depth was governed by the ice-water boundary. Deeper equatorial valley networks may result from latitudinal variations in the availability of water or formation efficiency.

Introduction

Martian valley networks are frequently cited as the best evidence that liquid water once flowed over the surface of Mars [e.g. Carr, 1996; Baker *et al.*, 1992]. While the fluvial origin is generally accepted, controversy remains over the relative role of various formation processes including ground water sapping [Sharp and Malin, 1975; Pieri, 1980; Howard *et al.*, 1988; Goldspiel and Squyres, 2000], surface runoff [Baker and Kochel, 1979; Gulick and Baker, 1990] and ground water flow resulting in subsurface solution and erosion [Malin and Carr, 1999; Carr and Malin, 2000]. In addition, the role of liquid water in the formation of valley networks has led to the suggestion that Mars may have had a warmer and wetter climate in the past. Researchers have proposed that valley networks largely formed during an early period in martian history with a more clement climate [Sagan *et al.*, 1973; Pollack, 1979; Carr, 1981]. Baker *et al.* [1991] advocate repeated, short-term warm climate periods occurring throughout martian history. Thus, understanding the timing and formation processes for valley networks is important for deducing past martian climatic conditions.

The high resolution topographic data set from the Mars Orbiter Laser Altimeter (MOLA) [Zuber *et al.*, 1992; Smith *et al.*, 1999] on the Mars Global Surveyor (MGS) spacecraft [Albee *et al.*, 1998] affords the opportunity to study the morphometry of valley networks in detail. Although Goldspiel *et al.* [1993] conducted a photoclinometric study of morphometry for 45 representative valley networks, the present study is the first to examine a global data set of valley network measurements. The primary goal of this study is to employ MOLA data to determine quantitatively valley network shape and examine changes in morphometry as a function of geographical location. Characterization of valley network morphometry is important in

determining the geologic, hydrologic and climatic conditions required for formation, and our morphometric data base is interpreted in terms of models for valley network origin.

Background

Nearly all valley networks cut Noachian terrain in the southern highlands [*Pieri, 1976*] and are concentrated within the older parts of the densely cratered terrain [*Carr and Clow, 1981*]. However, some valley networks are found on younger volcanic terrains or in regions with steep slopes, such as impact craters [*Gulick and Baker, 1990; Craddock and Maxwell, 1993*]. This distribution implies that most valley networks formed early in martian history, probably during the Noachian era [*Carr and Chuang, 1997*] and is consistent with the model of an early warm, wet Mars with high erosion rates that transitioned to a cold, dry planet with minimal erosion rates [*e.g. Carr, 1992; Craddock and Maxwell, 1993; Golombek and Bridges, 2000*]. While there is general agreement that water was involved in the formation of valley networks [*Mars Channel Working Group, 1983; Carr, 1996*], debate continues over the style of erosion (sapping, surface runoff, ground water discharge, solution, etc). It has long been noted that valley networks broadly resemble terrestrial drainage systems. Like terrestrial river valleys, valley networks are narrow and often have sinuous reaches with branching tributary systems (quasi-dendritic form). However, many valley network attributes suggest an alternate or complementary process to surface fluvial activity: U-shaped profiles, uniform top width over long distances, cliff-like walls, rounded amphitheater terminations to tributaries, patterns of branching and rejoining, lines of closed depressions extending beyond valley head [*Carr and Malin, 2000*], the lack of channel bedforms, and low drainage densities for valley networks [*Carr and Chuang, 1997*] relative to terrestrial fluvial environments.

Formation Processes

The extreme variations in valley network cross-sectional profile shape (V- to U-shape) and planimetric form (quasi-dendritic to long, sinuous valleys with a few, short amphitheater-termination tributaries) suggest that valley networks are complex landforms that likely resulted from multiple processes. Further, the preservation state of valley networks also varies and the same network may contain both pristine and degraded segments [*Baker and Partridge, 1986; Carr and Malin, 2000*]. A variety of formation processes have been proposed and are briefly described below. Note that all of the mechanisms below, except 1b, require a climate more suitable to the stability of surface or near-surface water than the present arid, frigid climate.

1) *Surface Runoff*.

- a) *Fluvial surface runoff* [*Sharp and Malin, 1975*]. Fluvial activity deriving from precipitation or ground water aquifers is consistent with the observed quasi-dendritic valley network shape and sinuous character of some networks. While precipitation was unlikely to have been directly responsible for carving the valley networks because of the observed low drainage density [*Carr and Chuang, 1997*] and lack of small-scale valleys (less than 100 m wide) in Mars Orbiter Camera (MOC) images [*Malin et al., 1992; Carr and Malin, 2000*], it may have aided their formation by recharging the ground water system [*Squyres, 1989a*]. Recharge by basal melting at the pole and transport of the meltwater through a global, interconnected megaregolith from the pole to the equator has also been proposed [*Clifford, 1993; Clifford and Parker, 2001*]. MOC observations of fresh-appearing valleys with V-shaped profiles and inner channels in regions suggest formation by sustained or episodic flow across the surface emanating from a ground water or surface runoff (i.e., precipitation) source.

b) *Fluvial, ice-covered* [Wallace and Sagan, 1979; Carr, 1983]. Under current climatic conditions, small-scale streams would freeze rapidly. Detailed thermodynamic modeling has demonstrated that an ice cover can enable small-scale flows to survive long enough for the channels to form. However, concern persists that the development of icings within the stream would quickly retard flow as is observed in spring-fed streams in terrestrial sub-zero temperature environments [Sloan *et al.*, 1976; Williams and Smith, 1989; Carr, 1983].

2) *Sapping.*

a) *Ground water sapping.* Sapping refers to a process whereby ground water discharges to the surface at a point of geological control (i.e., joint or fault) and undermines the overburden to generate headward erosion at its point of emergence [e.g. Dunne, 1980, 1990]. This mechanism is consistent with the amphitheater terminations of tributaries, the U-shape cross-sectional shape and the relatively constant width from source to outlet [Laity and Malin, 1985]. The resulting debris is removed via fluvial processes.

b) *Geothermal sapping* [Squyres, 1989b]. Seepage erosion would be focused at the ice/water interface (273 K isotherm). The depth to the base of the cryosphere (melting isotherm), z_c , can be calculated from

$$z_c = K(T_{mp} - T_{ms}) / q \quad (1)$$

where K is the thermal conductivity of the cryosphere, q is the surface heat flux, and T_{mp} and T_{ms} are, respectively, the melting point temperature of ice and the local mean annual surface temperature [Fanale, 1976]. Based on current mean annual surface temperature, estimated values for geothermal heat flow [$\sim 30 \text{ mW m}^{-2}$] [Schubert *et al.*, 1992], thermal conductivity ($2.0 \text{ W m}^{-1} \text{ K}^{-1}$), and melting temperature, the depth to the base of the

cryosphere at present varies from ~2.3-3.7 km at the equator to approximately ~6.5-8 km at the poles [*Clifford and Hillel*, 1983; *Clifford and Parker*, 2001]. Thus, there is a poleward increase in the depth to the base of the cryosphere reflecting the latitudinal decline in mean annual surface temperature. As geothermal heat flux was greater in the past [e.g. *Stevenson et al.*, 1983; *Schubert et al.*, 1992], the cryosphere thickness must have increased with time. *Clifford and Parker* [2001] use present mean annual surface temperature to estimate the depth to the base of the cryosphere at 4 Ga to be ~0.5-0.7 km at the equator and ~1.3-1.6 km at the poles. Regardless of absolute depth, the geothermal sapping hypothesis implies that the deepest valley networks should be located at higher latitudes where the depth to the ice/water interface is greatest.

- 3) *Water-lubricated mass wasting* [*Carr*, 1995]. In this model, the channel forms as a result of slope failure primarily at the head, but also on the channel walls. Headward erosion by ground water sapping may have aided the dominant mass wasting process. Ground water seepage mobilizes the debris and creates a slow moving (cm/yr) debris flow. MOC observations of gullies developed on crater walls show fill apparently derived from the walls of the gully and striae indicating material was transported downslope within the gully [see Figure 12a in *Carr and Malin*, 2000]. While it is unclear whether this mass wasting process formed the gully or resulted from the presence of the gully, MOC examples showing similar evidence for mass processes in valley development are rare indicating that this model is unlikely to be the dominant valley network formation process.
- 4) *Ground water flow* [*Carr and Malin*, 2000]. MOC images of valley networks reveal sinuous sections and discontinuous lines of closed depressions sections in Hephaestus Fossae and Hebrus Vallis. *Carr and Malin* [2000] interpret these observations as evidence for massive,

channelized, subsurface flow of water resulting in either erosion (piping) of loose friable material or, more likely, solution.

Methodology

This study builds upon the valley network GIS database compiled by Carr [1995] in ARC/INFO [Environmental Systems Research Institute, 1992]. The database catalogs more than 9000 valley network segments including more than 800 individual systems. The attribute file for each feature includes parameters such as latitude, longitude, length, stream order and maximum age (defined as the youngest geologic unit a valley network cuts). MOLA has a spot size of 150 m in diameter and a footprint-to-footprint spacing of ~300 m along track with a vertical precision of ~30 cm [Smith *et al.*, 1998]. A search algorithm is used to identify which valley networks are sampled by MOLA for a particular MGS orbit. For each valley network crossing, morphometric measurements of valley network depth, top width, bottom width, and minimum elevation are derived from the MOLA dataset and then incorporated into the database. The same measurements are made for interior channels, where observed. In addition, parameters detailing the orientation of the groundtrack with respect to the valley network strike are also included so that an estimate of the true local cross-sectional parameters can be made from each oblique crossing. This study excluded measurements from orbits that had a near parallel (<15°) alignment with valley network strike.

Figure 1 illustrates an asymmetric valley network profile where the valley walls have different heights and provides a useful example to define the measurements made. Top width (W_T) is measured as a horizontal line from the lowest valley rim across the valley to the adjacent wall. Bottom width (W_B), when resolved in the MOLA profile, is the relatively horizontal

portion of the profile covering the valley floor. Valley depth (D) is the difference between average wall elevation and minimum channel elevation.

Results

This study examines 1868 MOLA crossings of valley networks acquired through the first three months of mapping data. Valley networks have been identified on a variety of geologic terrains, and the database samples valley networks in all of the regions where they are located (Figure 2). The measurements are concentrated on the southern highland terrain where valley networks primarily occur. Table 1 summarizes our quantitative assessment of valley network morphology. The distribution of valley top width, depth, and top-width-to-depth (F) measurements are distinctly unimodal as illustrated in Figure 3. The standard deviation of the mean for both top width and depth is skewed by the small fraction of wide (>4 km) and deep (>200 m) valley networks. Interior channels were extremely rare ($<1\%$) in our observations. Thus, the characteristic valley network shape is a few kilometers in width and 100 m deep with corresponding top-width-to-depth ratios (F) between 13 and 37. Figure 4 illustrates that valley top widths are correlated with valley depths up to approximately 125 m depth and this correlation is reasonably approximated by a straight-line fit; this encompasses a majority ($\sim 77\%$) of the valley network measurements within the study. (Extremely atypical valley networks with depths >275 m, comprising 4% of the database, were not included in this analysis.) At depths greater than ~ 125 m, average top width values deviate from the straight-line fit. Valley network shape, as characterized by the top-width-to-depth ratio, F , shows a distinct decline as a function of depth (Figure 5). Thus, as valley networks become deeper, their aspect ratio declines.

Also, the data set was examined for any latitudinal dependence of morphometry. Figures 6a and 7a are plots of mean top width and depth, respectively, in 5° latitude bins. The larger

error bars in the northern hemisphere stem from the lower occurrence of valley networks there. Despite the scatter in these plots, it appears that both width and depth decrease with increasing latitude, particularly in the southern hemisphere. To evaluate these observations, a t -statistic was used to test the null hypothesis that the means from adjacent 20° latitude bins are the same [e.g. *Wadpole and Myers, 1985*]. The two-tail P -value is the probability that, assuming the null hypothesis is true, randomly selected samples would have means as far apart as those observed with either group having the larger mean. P -values less than 0.05 provide strong evidence that the difference between the two populations is real (only 1 in 20 chance that observed difference in means is due to chance) [*Kitchens, 1987*]. There is a statistically significant narrowing of the valley network top width by approximately 0.5 km at higher southern latitudes and low northern latitudes, relative to equatorial valley networks (0° latitude bin) (Figure 6b). The small P -values obtained in comparing the depth bins (Figure 7b) indicates that the population means are different (i.e. the null hypothesis is rejected) at the 95% confidence level. From Figure 7b, it is observed that mean depth decreases by approximately 50 m from the equator to higher latitudes ($\pm 50^\circ$).

In addition, the characteristics and geographical distribution of U- and V-shape valleys was examined. Valley shapes were classified as V-shape (profile comes to a distinctive point) or U-shape (at least two MOLA shots at approximately the same elevation indicative of a flat-floor). Approximately 60% of the cross-sections within the database had a V-shape profile. The average U-shape valley is 18 m deeper and 1313 m wider than the average V-shape valleys. Again, the t -statistic was employed to examine latitude correlations for V- and U- shape valleys, as described above. In the V-shape case, a pronounced narrowing (~ 520 m) of top width for valleys at high latitudes was noticed relative to the equatorial valleys (Figure 8a). This result is

consistent with that obtained for the entire data set (Figure 6b). However, top width does not show any latitude dependence in the U-shape case (Figure 8b). The two-tailed t -statistic results indicate the null hypothesis (the mean top width is the same in comparing all latitude bins in the U-shape case) is accepted at the 95% confidence level. Figure 9a illustrates that V-shape valleys also exhibit the decrease in depth (~ 75 m) between the equator and higher latitudes observed in the entire data set (Figure 7b). However, in the U-shape case (Figure 9b), the null hypothesis that the mean depths are the same between -30° and 30° latitude is accepted at the 95 % confidence level based on the two-tailed t -statistic results. There is a statistically significant decreases in mean depth between the equator and the highest latitude bin ($\pm 40^\circ$), however, the magnitude is ~ 30 m to the south and ~ 75 m to the north. Thus, the U- shape valleys do exhibit shallower average depths at high latitudes relative to equatorial U-shape valleys. In summary, V-shape valleys exhibit the depth and top width latitude dependence observed in the entire dataset while the U-shape valleys only display the decrease in depth at higher latitudes relationship.

Finally, the distribution of U- and V-shape valleys within a single network was examined. In 41% of the networks sampled in this study, both U- and V- shapes occurred within the same system. *Baker and Partridge* [1986] made the observation that U-shape valleys are preferentially found in the downstream reaches and V-shape valleys are typically located in the upstream reaches of a valley network system and they advocate the following formation scheme to explain the distribution of cross-sectional shape within the same valley network system: 1) development of valley networks via overland flow runoff which yields a V-shape cross-sectional valley shape; 2) formation of the intercratered plains, which may have partly buried the valley networks by lava flows and sedimentation; 3) reactivation of the valley networks by headward

sapping processes producing the pristine, U-shape valley networks which 4) cease formation at approximately the termination of the heavy bombardment (3.8-3.9 bya). The last two steps occurred very rapidly and are constrained to a 1×10^8 year window by crater counts between the densely cratered terrain and the intercratered plains. As a test case, the valley network shape derived from MOLA crossings of the Loire Valles system that originates in the Parana Basin of Margaritifer Sinus were examined (Figure 10). This example illustrates the relationship of U-shape predominantly located in the trunk of the system (branches with high stream order) and V-shape profiles located on tributaries (branches with low stream order) and in the upstream section and supports the observations made by *Baker and Partridge* [1986]. Additional investigation of the distribution of V- and U-shape valleys within network systems should be undertaken in the future and awaits further collection of data to increase the number of profiles within a single system (within the present database, the vast majority of networks have less than 5 data profiles).

Assessment of Post-Formation Modification of Valley Networks

Post-formation channel modification may have altered the original valley network shape. Subsequent aeolian deposition or mass wasting infilling would yield a shallowing of valley networks. Widening of the channels after formation could occur through weathering and mass wasting processes. Thus, the measured depths are minimum and the widths are maximum estimates of unmodified valley network values. In order to assess the usefulness of the measured morphometric parameters for evaluating valley network genesis, the degree of post-formation valley network morphometric alteration must be assessed.

The presence of dunes in topographic lows on Mars suggests that wind blown material has affected valley network depth [*Breed et al.*, 1982; *Ward et al.*, 1985]. High resolution MOC images of valley networks confirm the presence of dunes in many valley networks. Further,

aeolian deposition has been invoked to explain the lack of observed interior channels within valley networks [Malin and Carr, 1999] and the observed flat-floored profile of some valleys [Carr and Malin, 2000]. However, Goldspiel *et al.* [1993] estimate less than 20 m of aeolian infill based on small crater rim heights preserved on valley network floors. Furthermore, the hypothesis that the observed depth decrease as a function of latitude (Figure 7) is the result of a latitude-dependent sedimentation process can be evaluated through examination of the change in top-width-to-depth ratio, F , as a function of latitude (Figure 11). For the V-shape case, both width and depth decrease with higher latitude to preserve constant F (Figures 8, 9 and 11). Evolution scenarios that could produce this observation are labeled ambiguous in Table 2. The fortuitous filling as a function of latitude to transform valleys that initially formed with F varying as a function of latitude to a uniform F value is doubtful. Thus, the simplest explanation is that F was constant as a function of latitude at the time of V-shape valley development. To preserve the constant F as a function of latitude would require either fill to decrease as a function of latitude or minimal modification of the valley shape by infilling. In the U-shape valleys, F increases as a function of latitude (Figure 11). If this relationship is due to infill, then either the amount of sedimentary fill will increase or be constant as a function of latitude (Table 2). Notice this is contrary to the V-shape case (decrease in fill as latitude increases) and we expect sedimentary fill processes to affect V- and U-shape valleys in the same manner. Thus, this analysis indicates that modification of valley shape by sedimentary infill is unlikely and this reinforces the contention that post-formation aeolian sedimentation in valley networks was minimal.

Infilling could also result from mass wasting processes whereby rock is dislodged and transported downslope under the influence of gravity. Given the relatively large widths of

valleys (few kms), the debris shed is likely to remain concentrated near the valley walls and may not have had a significant effect on maximum valley depth. MOC images do show talus slopes meeting at the center of the valley in fresh-appearing systems; however, for wide valley networks, the talus aprons do not meet in the center, but are confined near the walls [*Carr and Malin, 2000*]. In addition, MOC images show small dark streaks on valley slopes associated with fine-scale mass movement that would not significantly affect valley shape. Furthermore, as will be demonstrated in the next section, average valley wall slope increases with depth, which is contrary to mass wasting processes that result in a reduction in wall slope. Thus, if the observed steepening of wall slopes with depth is a primary feature associated with valley network formation, it suggests that mass wasting processes have not greatly altered the original valley shape.

Several observations suggest that landforms in the mid-latitudes were modified by water, in liquid or frozen form. 1) Rounded and subdued surface features, particularly within craters, in the 30° - 60° latitude belts, have been interpreted to be the result of terrain softening as the result of ice-abetted creep of mass-wasted debris [*Squyres and Carr, 1986*]. 2) Lobate debris aprons, interpreted to be analogous to terrestrial rock glaciers, are also found in 25° bands centered at 40° N and 45° S [*Squyres, 1978, 1979*]. Ground ice to produce softened terrain and debris flows may be the result of precipitation from the atmosphere [*Squyres, 1979*] or derived directly from the ground [*Lucchitta, 1984*]. 3) High resolution MOC images show gullies on cliffs and crater walls at mid- to high-latitudes (30° - 70°) interpreted as caused by seepage-fed surface runoff recently in martian geologic history (<1 million years ago) [*Malin and Edgett, 2000*]. 4) Furthermore, theoretical models predict the presence of near-surface ground ice in the mid- to high-latitudes [*e.g. Farmer and Doms, 1979; Clifford and Hillel, 1983; Fanale et al., 1986*]. The

most problematic aspect of this hypothesis is the lack of morphological expression indicating that ice-abetted creep preferentially modified mid-latitude valleys over near-equatorial valley networks. Unlike the fretted terrain, valley network floors do not show longitudinal striae, compressional ridges where opposing debris aprons meet or lobate terminations. While modification of valley networks by ice or water-lubricated debris flows can not be excluded, we are troubled by the lack of apparent distinction in landform style between equatorial and mid-latitude valley networks and the lack of diagnostic landforms suggesting water mobilized debris flows.

As noted earlier, varying degrees of preservation of valley networks have been documented. *Baker and Partridge* [1986] mapped 25 valley network systems at a 1:2,000,000 scale and recognized that both degraded and pristine sections are present within the same network complex. They characterize degraded sections as valleys that have scalloped or rilled valley walls, indistinct valley widths, and low slope angle on valley walls. The degraded valley networks were preferentially found in the headward areas of the network system on densely cratered terrain and were often separated from the pristine sections by knickpoints. The pristine sections were described as U-shape, have theater-like head tributaries and were preferentially found downstream of degraded sections on younger, intercratered plains. *Baker and Partridge* [1986] see evidence of minimal degradation of valley networks after the formation period (i.e. post heavy bombardment), an observation consistent with the rapid decline in erosion rates since the Noachian [*e.g. Golombek and Bridges, 2000*].

Based on the reasons given above, the measured morphometric parameters reported here are interpreted to be representative of the valley network shape at the time of formation. While

post-formation modification of valley network systems has undoubtedly occurred, the valley morphometry is dominantly due to channel formation mechanisms.

Model of Valley Network Shape

Valley network shape, defined as the top width to depth ratio, F , decreases as valley networks get progressively deeper (Figure 5). In an effort to elucidate the conditions of valley network genesis, model cross-sections were constructed at several depths. The model used the derived linear relationships between measured variables to produce characteristic profiles for the two end-member case of flat-bottomed (U-shape) and V-shape cross-sections. For the V-shape end member case, top width, W_T , versus depth, D , exhibits the same deviation from the straight-line fit at depths greater than ~ 125 m observed in Figure 4, which incorporated the entire data set. Therefore, weighted linear regression lines were determined separately for binned data (binsize is 25 m) below (Equation 2) and above 125 m (Equation 3). Correlation coefficients, R , and standard error of regression, $\hat{\sigma}$, are given below, for the associated equations.

$$\begin{aligned} W_T &= 821.8 + 11.1D \\ R &= 0.96 \quad \hat{\sigma} = 156.7 \text{ m} \end{aligned} \quad (2)$$

$$\begin{aligned} W_T &= 1559.1 + 3.5D \\ R &= 0.63 \quad \hat{\sigma} = 240.8 \text{ m} \end{aligned} \quad (3)$$

For the V-shape end member case, average wall slope, θ , is computed by the relationship in Equation 2.4:

$$\theta = \tan^{-1} \left(\frac{D}{W_T / 2} \right) \quad (4)$$

For the flat-floored (U-shape) case, 532 measurements of valley networks with bottom widths, W_B , detectable in the MOLA profile were extracted. Again, there are deviations from the

straight-line fit in plots of top width, W_T , and change in width, ΔW , as a function of binned depth (binsize is 25 m) at depths greater than ~ 125 m. Therefore, weighted linear regressions were derived separately for data below (Equations 5 and 7) and above (Equations 6 and 8) this value.

$$\begin{aligned} W_T &= 1206.6 + 18.8D & (5) \\ R &= 0.99 & \hat{\sigma} = 68.5 \text{ m} \end{aligned}$$

$$\begin{aligned} W_T &= 1100.5 + 13.3D & (6) \\ R &= 0.74 & \hat{\sigma} = 566.2 \text{ m} \end{aligned}$$

$$\begin{aligned} \Delta W &= 695.9 + 11.1D & (7) \\ R &= 0.99 & \hat{\sigma} = 52.6 \text{ m} \end{aligned}$$

$$\begin{aligned} \Delta W &= 193.2 + 11.4D & (8) \\ R &= 0.82 & \hat{\sigma} = 427.3 \text{ m} \end{aligned}$$

where ΔW is defined as

$$\Delta W = W_T - W_B \quad (9)$$

In the U-shape case, the equation for average wall slope is modified to

$$\theta = \tan^{-1} \left(\frac{D}{\Delta W / 2} \right) \quad (10)$$

The calculated values for model valley network shape derived from the relationships given above are summarized in Table 3 and illustrated in Figure 12. For both cases, average wall slope, θ , increases with increasing depth. That is, the wall slopes are the steepest in the deepest valley networks. In addition, the width-to-depth ratio, F , decreases with depth in both cases. Relative to V-shape profiles, the U-shape profiles have larger F value at a given depth.

Figure 13 illustrates individual MOLA profiles that approximately match the derived model valley network shape. These profiles illustrate a steep break in slope at the valley rim which coincides with bedrock outcrops [Carr and Malin, 2000]. Further, they show generally

smooth valley walls at MOLA resolution. In roughly 40% of the MOLA profiles examined, concavities near the valley floor where wall slopes shallow were observed (i.e. footslope) which may be the result of small scale mass movements producing a talus slope (for example, see right bank of Figure 13F). These talus slopes likely formed after valley network formation ceased, but are relatively small-scale features that have not affected the measured depth or top width (Figure 1). Generally, these concavities were observed on only one side of the valley and did not extend to the valley center; thus the measured depth is unchanged. However, their location close to the floor may result in an under-estimation of bottom width for U-shape profiles.

An evolutionary relationship may exist between U- and V-shape valleys. Flat-bottom floor valleys may have originally formed with a V-shape profile and were subsequently filled with sediments to produce the observed flat floor (Figure 14a). This hypothesis is supported by the MOC observation that the flat floors of valley networks are not flood plains, but are interpreted as primarily the result of later aeolian fill [*Carr and Malin, 2000*]. To explore this hypothesis, the wall slopes of U-shape valleys were extrapolated down to the apex in order to approximate the proposed original valley shape (Table 4). The results of this analysis still demonstrates F decreasing with increasing depth, although the F values are larger than comparable V-shape F values for a given depth. Extrapolating the U-shape valley wall slopes results in an original depth that is too shallow, compared to what is expected if the U-shape originally had the same cross-sectional shape as V-shape valleys. Further, this hypothesis was tested by examining the latitude dependence of top width for U and V-shape valleys. Proposed sedimentary infilling of valleys would not affect the top width and thus, we would expect that both U- and V-shape valleys preserve the observed decrease in top width as latitude increases (Figure 6). However, only the V-shape profiles exhibit a narrowing of top width for valleys at

high latitudes relative to those located near the equator (Figure 8). Based on the results from these two tests, the hypothesis that U-shape valleys were originally formed with a V-shape and later sediment fill resulted in the observed flat-bottom floor is rejected. Aeolian fill itself does not explain the flatness observed within U-shape valley. Furthermore, this analysis suggests that aeolian fill has had only a minor influence on valley shape and is consistent with the estimated <20 m of aeolian fill by *Goldspiel et al.* [1993]. U-shape valleys appear to be formed from a different set of processes than the V-shape valleys.

Alternatively, the V-shape valleys could evolve into U-shape valleys through valley widening (Figure 14b). To extrapolate the original V-shape, the bottom width of U-shape valleys was minimized to a point while maintaining the observed wall slope, θ . Table 5 reports the derived original top width, W_{Torig} , and original width-to-depth ratio, F_{orig} , for the extrapolated V-shape. Comparison between F_{orig} and F_V (from Table 3) illustrates an overall agreement. The derived F_{orig} values are lower for depths less than 150 m than the observed F_V values. This is likely attributed to the fact that valley widening process may also have increased the depth. Thus, we conclude that widening of V-shape valleys to produce U-shape valleys is a viable hypothesis.

Discussion

Interpretation of Valley Network Shape

For both V- and U-shape valleys, it is assumed that the modeled valley shape as a function of depth represents a development continuum, where the deeper valley would generally result from a more advanced stage of the same process or processes that form the shallow valley (Figure 12). The results of the model include lower F values (the valleys get deeper faster than they get wider) and steeper wall slopes at greater depths. Fully 41% of the networks examined

had both U- and V-shape profiles within the same network system. However, there are notable differences between U- and V-shape profiles which suggests that certain processes may have been more dominant in the formation of U-shape profiles relative to their V-shape counterparts. The average U-shape profile is slightly deeper and significantly wider than the average V-shape profile (Table 1). Further, the top width of U-shape valleys does not exhibit the latitude correlation observed for the V-shape valleys (Figure 8). Perhaps most revealing is the fact that by narrowing the current U-shape valley until the bottom width goes to zero while maintaining the wall slope results in a width to depth ratio, F , similar to the V-shape valleys for the same depth (Table 5). Collectively, these results suggest that U-shape valleys developed with more valley widening relative to V-shape valleys, suggesting that side-wall sapping may have been an important process in the development of the U-shape profile.

These results are consistent with the *Baker and Partridge* [1986] model where V-shape valleys form via surface overland flow processes and U-shape valleys form secondarily through re-activation of the same valleys by headward extending sapping processes (see their Figure 10). According to this model, vertical incisement is the primary determinant of the valley depth. In these original V-shape valleys, the depth of incision controls the top width (Figure 4) and would yield a constant top-width-to-depth ratio, F , as a function of latitude (Figure 11). Secondary sapping processes affecting the lower portion of the drainage network would principally result in valley widening (particularly via side-wall sapping), a minimal increase in valley depth and a U-shaped valley. Given the initial constant F as a function of latitude for V-shape valleys, the sapping processes that widen the valley to produce U-shape valleys would result in higher F values as latitude increases (Figure 11) if widening was constant with latitude (Figure 8b). This mechanism requires a high water table and recharge is necessary to sustain sapping. The

formation of valley networks ceased at the end of the heavy bombardment period presumably due to a lowering or freezing of the water table. Small-scale mass wasting has occurred since valley network formation as evident by small dark streaks on valley walls in MOC images; however, this process has not affected valley width. Finally, aeolian infilling has occurred, resulting in small scale (<20 m) aeolian mantles and dune fields on many valley network floors.

The observation that average valley wall slopes increase with *depth* indicates wall slope steepening with *time* if shallower valley networks are examples of deeper valley networks earlier in their development. Several models of mass wasting have been documented on the Earth (slope decline, parallel slope retreat, etc.); however, all of them result in a maintenance or a decrease in wall slope with time [*e. g. Young, 1969*], contrary to our inferred steepening of wall slopes with time on Mars. Wall steepening with time could develop if the rate of vertical incisement is much faster than the rate of lateral erosion, a scenario consistent with the observed decrease in F with depth (Figure 12). These conditions are present in surface overland flow processes (the first phase of valley network development in the *Baker and Partridge [1986]* model). Alternatively, undermining of the valley walls is a mechanism that would result in steeper wall slopes with depth. Clearly, side-wall sapping would steepen wall slopes in the downstream U-shape reaches during the second phase of valley network development in the *Baker and Partridge [1986]* model. In the proposed earlier phase of surface flow runoff, several scenarios could lead to lateral erosion in the upper reaches of the valley network system. (1) As a stream gets close to base-level, vertical incisement slows and a larger percentage of the stream's energy is converted into lateral erosion. (2) Lateral erosion can be enhanced by high discharges where the stream energy suddenly increases, as would occur in flood conditions. (3) Surface flow may have encountered an impermeable, resistant, competent unit at depth and flow

would begin to undermine the wall stability by lateral erosion leading to wall collapse. This later scenario is particularly appealing, as the presence of a basal, impermeable layer is necessary for the proposed, later-stage sapping phase.

This model, coupled with previous observations and inferences of valley networks, suggests constraints on the host material valley networks formed within. (1) MOC images reveal layering of valley walls [*Malin et al., 1998; Carr and Malin, 2000*]. (2) *Carr and Malin [2000]* make a compelling case that the lack of micro-dissection of the martian surface in MOC images can best be explained if the host rock is very permeable and infiltration rates are high. Further, terrestrial cases of low drainage densities (still 2-3 orders of magnitudes larger than the drainage densities observed in martian valley network systems) are associated with regions with a high infiltration capacity of the surface [*Ritter, 1986*]. (3) Material shed from the valley walls must readily break down to fine particles or be soluble so that discharge within the system was sufficient to remove this eroded sediment. If the rock breaks down to gravel-sized or larger particles, these armor the valley floor and arrest vertical downcutting [*Schumm, 1977*]. (4) Finally, massive, competent rocks favor vertical incisement over lateral erosion [*e.g. Morisawa, 1968*]. The candidate rock units that meet all of these conditions are fractured basalt or indurated volcanic ash/cinders, both consistent with inferred surface rock types [*e.g. Bandfield et al., 2000*].

Relationship of Valley Network Shape to Latitude

We observe a ~50 m decrease in mean valley depth from the equator to higher latitudes (Figures 7 and 9). The dependence of depth with latitude does not follow the predicted relationship implied by the geothermal sapping theory [*Squyres, 1989a*]. The depth of the 273 isotherm demarcates the pure ice-water boundary and, according to this theoretical model, this

boundary was proposed to be the parameter that primarily governed the sapping depth. Surface temperature decreases from the equator to the pole because of the latitudinal decrease in solar insolation. An increase in elevation from the equator to the south pole [Smith, *et al.*, 1999] adds to this effect in the southern hemisphere. Given a globally uniform surface heat flux, the depth to the 273 K isotherm would increase at higher latitudes, particularly in the southern hemisphere. Even accounting for infilling, as discussed above, the deepest valley networks are found near the equator. Thus, the geothermal sapping model is inconsistent with the MOLA observations.

A decrease in depth of valleys at higher latitudes relative to equatorial latitudes for both U- and V-shaped valleys is observed (Figure 9). However, only the V-shaped valleys exhibit a decrease in top width as latitude increases (Figure 8). These results make sense in terms of the two-phase valley network formation model of Baker and Partridge [1986]. The first phase of surface runoff produced the V-shape profile, and the depth of incision controlled the top width. In the second phase, sapping processes predominantly widened the valley, producing a U-shape. Thus, U-shape valleys preserve the latitude dependence of depth, but overprint the latitude dependence of width observed in V-shape valleys.

Several scenarios could explain the apparent latitude dependence of the surface runoff process (first phase). Changes in the orbital and rotational motions of Mars may have aided the existence of an early warmer and wetter climate and increased the effect of the seasons [Ward, 1992]. Seasonal effects affecting surface temperature as a function of latitude may have impacted valley network formation rates if surface runoff processes were involved. Thus, it is possible that near-equatorial valley networks could form year-round while the formation of valley networks at higher latitudes would slow or even cease for the half of the martian year during the cold season. Interestingly, near-equatorial valley networks are presently

approximately twice as deep as those found at higher latitudes which is suggestive of a doubling in formation rate at the equator. Furthermore, if valley networks formed under climatic conditions that were warmer and wetter than present, the change in climate may have resulted in a cessation of valley network formation at high latitudes before low latitudes. That is, as the climate transitioned to the current cold, dry state, the ground at high latitude could freeze first and arrest valley network formation while equatorial valley networks continued to form. Climate change models suggests that this freeze-out would take a couple hundred million years and would migrate from the poles to the equator [Carr, 1999]. Alternatively, assuming a thicker atmosphere was present during the Noachian, precipitation may have varied by latitude with the greatest accumulation in the near-equatorial region, possibly analogous to the precipitation pattern that is present on Earth. Thus, enhanced precipitation-fed recharge of the ground water system in the near-equatorial region may contribute to the formation of the deeper valley networks located there.

Conclusions

Analysis of valley network morphometry can provide insight into the conditions of formation. This study has demonstrated that the typical valley network shape is a few kilometers wide and ~100 m deep. The relatively shallow depth indicates that liquid water existed within a few hundred meters from the surface during the Noachian, if valley networks formed by any process involving water (sapping, ground water flow, surface runoff, water-lubricated mass wasting, etc.). The linear correlation of top width and depth may be an indication that the depth of vertical incision influenced the top width of the valley for the majority of valley networks (those with depths less than 125 m). Typical characteristics of valley network shape include steeper wall slopes and lower width-to-depth ratios, F , with increasing depth.

The hypothesis that U-shape valleys originally formed as V-shaped valleys and that their flat-floors are primarily the result of subsequent aeolian fill is refuted by the results of this paper. The model calculations yield a derived V-shape valley that is significantly shallower than would be expected based on measured V-shape valleys' width-to-depth ratio, F (Table 4). Therefore, the flat-floors of U-shape valleys presumably formed during valley network development. The differences in U- and V-shape valley characteristics must be accounted for by a variation in the formation mechanisms. Flat-floored (U-shape) valleys have characteristics that differ from V-shape valleys: (1) U-shape valleys are deeper and wider, and (2) U-shape valleys do not exhibit decreasing top width with higher latitudes, a characteristic of V-shape valleys. These observations are consistent with a two-phase model of valley network development proposed by *Baker and Partridge* [1986]. Wall undermining by lateral erosion or side-wall sapping may have occurred during both phases. Small-scale mass wasting and aeolian deposition has occurred since formation, but has minimally affected the original valley network shape.

Equatorial valley networks are approximately 50 m deeper relative to those at higher latitudes. This MOLA observations are contrary to the predicted relationship based on theoretical arguments from the geothermal sapping model indicating that the depth of sapping is not controlled by the depth to the ice-water boundary [*Squyres*, 1989b]. Factors that may result in deeper valley networks include the availability of water, increased formation efficiency or increased formation time at the equator. Seasonal cycles, possibly amplified by orbital and rotational motions of the planet, may also explain why V-shape valley networks, presumably formed by surface runoff, are roughly twice as deep as high latitude valley networks. These observations are also consistent with greater precipitation-fed recharge of the ground water

system at the equator relative to higher latitudes. Alternatively, climate change progressively freezing the ground from high to low latitudes may have inhibited valley network formation at high latitudes while near-equatorial valley networks continued to deepen for several hundred million years.

Future research can expand upon the results presented here. Of fundamental importance is an exploration of the relationship between valley network morphology and planimetric form to geologic terrain, a topic beyond the scope of this study. In addition, while we have examined the global patterns of valley network morphometry, future work should focus on individual network systems through an examination of MOLA and MOC data to test further the two-stage formation model advocated here.

Acknowledgements: We are grateful to Michael Carr for sharing his valley network database with us. Special thanks are extended to Amanda Heuremann and Elizabeth Miller for assistance in data collection, C. David Brown for software and Greg Neumann for MOLA data analysis, reduction and management. This paper was greatly improved by a constructive review from Goro Komatsu and useful discussions with Ray Arvidson. This research was supported by NASA Grant NAG5-4435.

References

- Albee, A. L., Palluconi, F. D., and Arvidson, R. E., Mars Global Surveyor mission: Overview and status, *Science*, 279, 1671-1672, 1998.
- Baker, V. R., et al., Ancient oceans, ice sheets and hydrological cycle on Mars, *Nature*, 352, 589-594, 1991.
- Baker, V. R., et al., Channels and valley networks, in *Mars*, edited by Kieffer, H. H., et al., pp.493-522, Univ. of Ariz. Press, Tucson, 1992.
- Baker, V. R. and R. C. Kochel, Martian channel morphology: Maja and Kasei Valles, *J. Geophys. Res.*, 84, 7961-7983, 1979.
- Baker, V. R. and Partridge, J. B., Small martian valleys: Pristine and degraded morphology, *J. Geophys. Res.*, 91, 3561-3572, 1986.
- Bandfield, J. L., Hamilton, V. E., and P. R. Christensen, A global view of Martian surface compositions from MGS-TES, *Science*, 287, 1626-1630, 2000.
- Breed, C. S., McCauley, J. F. and M. J. Grolier, Relict drainages, conical hills, and the eolian veneer in southwest Egypt—Application to Mars, *J. Geophys. Res.*, 87, 9929-9950, 1982.
- Carr, M. H., *The Surface of Mars*, 232 pp., Yale University Press, New Haven, 1981.
- Carr, M. H., The stability of streams and lakes on Mars, *Icarus*, 56, 476-495, 1983.
- Carr, M. H., Post Noachian erosion rates: Implications for Mars climate change, *Lunar Planety. Sci. Conf. XXIII*, 205-206, 1992.
- Carr, M. H., The Martian drainage system and the origin of networks and fretted channels, *J. Geophys. Res.*, 100, 7479-7507, 1995.
- Carr, M. H., *Water on Mars*, Oxford U Press, New York, 229 pp., 1996.
- Carr, M. H., Retention of an atmosphere on early Mars, *J. Geophys. Res.*, 104, 21,897-21,909,

- 1999.
- Carr, M. H., and F. C. Chuang, Martian drainage densities, *J. Geophys. Res.*, 102, 9145-9152, 1997.
- Carr, M. H., and G. D. Clow, Martian channels and valleys: Their characteristics, distribution and age, *Icarus*, 48, 91-117, 1981.
- Carr, M. H., and M. C. Malin, Meter-scale characteristics of martian channels and valleys, *Icarus*, 146, 366-386, 2000.
- Clifford, S. M., A model for the hydrologic and climatic behavior of water on Mars, *J. Geophys. Res.*, 98, 10,973-11,016, 1993.
- Clifford, S. M., and D. Hillel, The stability of ground ice in the equatorial regions of Mars, *J. Geophys. Res.*, 88, 2456-2474, 1983.
- Clifford, S. M., and T. J. Parker, The evolution of the martian hydrosphere: Implications for the fate of a primordial ocean and the current state of the northern plains, *Icarus*, (in press) 2001.
- Craddock, R. A. and T. A. Maxwell, Geomorphic evolution of the martian highlands through ancient fluvial processes, *J. Geophys. Res.*, 98, 3453-3468, 1993.
- Dunne, T., Formation and controls of channel networks, *Progress in Phys. Geography*, 4, 211-239, 1980.
- Dunne, T., Hydrology, mechanics, and geomorphic implications of erosion by subsurface flow, in Higgins, C. G., and Coates, D. R., eds., *Groundwater geomorphology*, GSA Spec. Paper 252, pp. 1-28, Boulder, Colorado, 1990.
- Environmental Systems Research Institute, *Understanding GIS*, Redlands, Calif., 1992.
- Fanale, F. P., Martian volatiles: Their degassing history and geochemical fate, *Icarus*, 28, 179-

- 202, 1976.
- Fanale, F. P., Salvail, J. R., Zent, A. P., and Postawko, S. E., Global distribution and migration of subsurface ice on Mars. *Icarus*, 67, 1-18, 1986.
- Farmer, C. B. and Doms, P. E., Global and seasonal variation of water vapor on Mars and the implication for permafrost, *J. Geophys. Res.*, 84, 2881-2888, 1979.
- Goldspiel, J. M. and Squyres, S. W., Groundwater sapping and valley formation on Mars, *Icarus*, 148, 176-192, 2000.
- Goldspiel, J. M., Squyres, S. W., and D. G. Jankowski, Topography of small martian valleys, *Icarus*, 105, 479-500, 1993.
- Golombek, M. P. and N. T. Bridges, Erosion rates on Mars and implications for climate change: Constraints from the Pathfinder lander site, *J. Geophys. Res.*, 105, 1841-1853, 2000.
- Gulick, V. C. and V. R. Baker, Origin and evolution of valleys on martian volcanoes, *J. Geophys. Res.*, 95, 14,325-14,344, 1990.
- Howard, A. H., Kochel, K. R., and H. E. Holt, Sapping features of the Colorado Plateau, NASA SP-491, 1988.
- Kitchens, L. J., *Exploring Statistics*, p. 331-333, West Publishing Company, St. Paul, 1987.
- Laity, J. E., and M. C. Malin, Sapping processes and the development of theater-headed valley networks in the Colorado Plateau, *Geol. Soc. Am. Bull.*, 96, 203-217, 1985.
- Lucchitta, B. K., Ice and debris in the fretted terrain, Mars. *J. Geophys. Res.*, 89, B409-B418, 1984.
- Malin, M. C., et al., Mars Observer Camera, *J. Geophys. Res.*, 97, 7699-7718, 1992.
- Malin, M. C. et al., Early views of the martian surface from the Mars Orbiter Camera of Mars Global Surveyor, *Science*, 279, 1681-1685, 1998.

- Malin, M. C., and Carr, M. H., Groundwater formation of martian valleys, *Nature*, 397, 589-591, 1999.
- Mars Channel Working Group, Channels and valleys on Mars, *Geol. Soc. Am. Bull.*, 94, 1035-1054, 1983.
- Morisawa, M., Streams: Their dynamics and morphology, McGraw-Hill, New York, 169 pp., 1968.
- Pieri, D. C., Martian channels: Distribution of small channels on the martian surface, *Icarus*, 27, 25-50, 1976.
- Pieri, D. C., Martian valleys: Morphology, distribution, age and origin, *Science*, 210, 895-897, 1980.
- Pollack, J. B., Climate change on the terrestrial planets, *Icarus*, 37, 479-553, 1979.
- Ritter, D. F., *Process Geomorphology*, p. 421, Wm. C. Brown, Dubuque, Iowa, 1986.
- Sagan, C., Toon, O. B., and Gierasch, P. J., Climate change on Mars, *Science*, 181, 1045-1049, 1973.
- Schubert, G., et al., Origin and thermal evolution of Mars in *Mars* edited by Kieffer, H. H., et al., pp. 147-183, Univ. of Ariz. Press, Tucson, 1992.
- Schumm, S. A., *The Fluvial System*, p. 106-111, John Wiley, New York, 1977.
- Sharp, R. P. and Malin, M. C., Channels on Mars, *Geol. Soc. Amer. Bull.*, 86, 593-609, 1975.
- Sloan, C. E., Zenone, C., and Mayo, I. R., Icings along the Trans-Alaska pipeline route *U. S. Geol. Surv. Prof. Paper 979*, 1976.
- Smith, D. E., et al., Topography of the northern hemisphere of Mars from the Mars Orbiter Laser Altimeter, *Science*, 279, 1686-1692, 1998. 1998.
- Smith, D. E., et al., The global topography of Mars and implications for surface evolution, *Science*, 284, 1495-1503, 1999.
- Squyres, S. W., Mars fretted terrains, flow of erosional debris, *Icarus*, 34, 600-613, 1978.

- Squyres, S. W., The distribution of lobate debris aprons and similar flows on Mars, *J. Geophys. Res.*, 84, 8087-8096, 1979.
- Squyres, S. W., Urey Prize Lecture: Water on Mars, *Icarus*, 79, 229-288, 1989a.
- Squyres, S. W., Early Mars: Wet, and warm, or just wet? *Lunar Planet Sci. Conf. XX*, pp. 1044-1045, 1989b.
- Squyres, S. W. and Carr, M. H., Geomorphic evidence of the distribution of ground ice on Mars, *Science*, 231, 249-252, 1986.
- Stevenson, D. J., Sphon, T., and G. Schubert, Magnetism and the thermal evolution of the terrestrial planets, *Icarus*, 54, 466-489, 1983.
- Wadpole, R. E. and Meyers R. H., Probability and Statistics for Engineers and Scientists, McMillan, New York, 1985.
- Ward, W. R., Long term orbital and spin dynamics of Mars, in *Mars*, edited by Kieffer, H. H., et al., pp. 298-320, Univ. of Ariz. Press, Tucson, 1992.
- Ward, W. R. et al., Global map of eolian features on Mars, *J. Geophys. Res.*, 90, 2038-2056, 1985.
- Wallace, D., and Sagan, C., Evaporation of ice in planetary atmospheres: Ice-covered rivers on Mars, *Icarus*, 39, 385-400, 1979.
- Williams, P. J. and Smith, M. W., *The Frozen Earth*, Cambridge University Press, Cambridge, 1989.
- Young, A., *Slopes*, Oliver and Boyd, Edinburgh, p.38-40, 1969.
- Zuber et al., The Mars Observer laser altimeter, *J. Geophys. Res.*, 97, 7699-7718, 1992.

Figure Captions

Figure 1: Topographic profile of valley network from orbit 10130 with MOLA shots marked by solid dots. Profile is not reprojected to correct for oblique crossing. Vertical exaggeration is 50X. Solid lines illustrate parameters measured: W_T = top width, W_B = bottom width, D = depth, X marks average wall height. See text for discussion.

Figure 2: Geographical distribution of 1868 MOLA profile measurements acquired in this study. The distribution of measurements corresponds to the distribution of valley networks, which are predominantly located in the southern highland terrain.

Figure 3: Frequency histograms of valley network morphometry illustrating the number of observations for each bin size. White box indicates interquartile range of data. Black line within box corresponds to median value and the edges of the box denote the median value of the first (first quartile) and last (third quartile) half of the ordered data set, respectively. a) Depth values with bin size 20 m. b) Top width values with bin size 250 m. c) Width to depth ratios (F) with bin size 5.

Figure 4: Top width versus depth plot. Plot incorporates 96% of the dataset due to exclusion of atypical valley networks with depths greater than 275 m. Data points correspond to mean depth value in 25 m depth bins. Error bars are 1 standard deviation of the mean. A weighted, least-squares straight-line fit is shown, with a corresponding correlation coefficient, R , of 0.96. The correlation coefficient measures the strength of the linear association between two quantitative

variables and ranges from 0 (no linear association) to ± 1 (perfect linear association) and is controlled by data with smaller error bars.

Figure 5: Plot of top width-to-depth ratio, F , versus mean valley depth, D , in 25 m depth bins illustrating induced correlation. Error bars are 1 standard deviation of the mean. A pronounced decline in F is associated with increasing valley network depth. Atypical depths greater than 375 m, comprising <2% of the database, were not included in this analysis. Equation was derived from weighted linear regression in Figure 3.

Figure 6: a) Mean top width values plotted for 5° latitude bins. Error bars are 1 standard deviation of the mean. b) Mean top width values plotted for 20° latitude bins. P -values denote probability that the two populations have the same mean value. Error bars are 1 standard deviation of the mean.

Figure 7: a) Mean depth values plotted for 5° latitude bins. b) Mean depth values plotted for 20° latitude bins. P -values denote probability that the two populations have the same mean value. Error bars are 1 standard deviation of the mean for both plots.

Figure 8: Mean top width values plotted for 20° latitude bins for a) valley networks with V-shape profiles and b) valley networks with U-shape profiles. Error bars are 1 standard deviation of the mean. P -values denote probability that the two populations have the same mean value.

Figure 9: Mean depth values plotted for 20° latitude bins for a) valley networks with V-shape profiles and b) valley networks with U-shape profiles. Error bars are 1 standard deviation of the mean. *P*-values denote probability that the two populations have the same mean value.

Figure 10: A) Viking image mosaic of Loire Valles, the valley network that emanates from the Parana Basin. MOLA measurements obtained in this study are denoted by open circles for U-shape profiles and black triangles for V-shape profiles. Only profiles for the central trunk of the system are illustrated. B-F) Cross-sectional profiles across valley networks (locations illustrated in A) have been re-projected to the plane perpendicular to the inferred flow direction. Cardinal directions are given at the top and orbit number is given at the bottom of each plot. Vertical exaggeration is 20X. In general, U-shape profiles are located in the downstream portions of the central channel while V-shape profiles are located in the tributaries (not shown) and in the upper reaches of the valley network.

Figure 11: Mean top-width-to-depth ratio, F , plotted in 10° latitude bins for V-shape (circles) and U-shape (diamonds) valley networks for the southern hemisphere. Error bars are 1 standard deviation of the mean.

Figure 12: Model-derived valley network cross-sectional profiles at various depths. Both V-shape and flat-bottomed floor profiles were modeled. As depth increases, the width-to-depth ratio, F , decreases in both cases.

Figure 13: MOLA topographic profiles of valley networks with shapes consistent with model-derived valley network shape. Each valley network has been reprojected to the plane perpendicular to valley network orientation. Vertical exaggeration is tenfold. Depth and width to depth ratio, F , is given for each profile in the header. MGS orbit number is in lower right corner. Approximate center latitude and longitude for each profile are as follows: A) -18.5° S, 87.8° E; B) -3.1° S, 130.3° E; C) -15.2° S, -18.27° E; D) -23.3° S, -10.35° E; E) -22.5° S, -9.34° E.

Figure 14: A) Schematic illustration of measured U-shape valley (black shape) extrapolated to a hypothetical original V-shape valley based on the measured average wall shape, θ , valley top width, W_T , and valley depth, D . The original V-shape valley depth, D_{orig} , is the sum of valley depth, D , and the depth of fill, D_{fill} . B) Schematic illustration of measured U-shape valley (unfilled trapezoid) extrapolated to a hypothetical original V-shape valley. The measured top width, W_T , is minimized until the bottom width reaches zero, forming the original V-shape valley (black triangle). Using the measured wall slope, θ , the original top width of the V-shape valley, W_{Torig} , can be determined.

Tables

Table 1: Morphometric Parameters of Valleys

		$\bar{x} \pm \sigma$	Median	Interquartile Range
All Valleys	Depth D (m)	109 ± 137	80	50 – 121
	Top Width W_T (m)	2040 ± 1548	1628	1005 – 2574
	Top Width-to-Depth F	29 ± 26	22	13 - 37
V- shape Valleys	Depth D (m)	102 ± 139	70	45 – 115
	Top Width W_T (m)	1721 ± 1352	1384	918 – 2123
	Top Width-to-Depth F	25 ± 34	21	13 – 35
U-shape Valleys	Depth D (m)	120 ± 122	95	65 – 135
	Top Width W_T (m)	3034 ± 1934	2624	1833 – 3818
	Top Width-to-Depth F	36 ± 23	30	19 - 48

Table 2: Evolution of valley shape as a result of fill processes

This analysis examines the effects of sedimentary fill processes given the original valley shape and modification scenario as a function of latitude. Valley top width is unmodified in time. Original conditions are the relationship of channel shape (top-width-to-depth ratio, F) as a function of latitude at the time of valley development. Modification scenario refers to the latitudinal distribution of fill. Notation within the table: \uparrow means increase, \downarrow means decrease, w/ means with, lat is latitude, const is constant. An ambiguous outcome occurs when the valley shape, F , could increase or decrease with increasing latitude. Note that for these situations, valley shape could evolve to have a uniform F as a function of latitude.

		Original conditions		
		F const w/ \uparrow lat	F \uparrow w/ \uparrow lat	F \downarrow w/ \uparrow lat
Modification Scenario	Const fill w/ \uparrow lat	F \uparrow w/ \uparrow lat	F \uparrow w/ \uparrow lat	F \downarrow w/ \uparrow lat
	Fill \uparrow w/ \uparrow lat	F \uparrow w/ \uparrow lat	F \uparrow w/ \uparrow lat	Ambiguous
	Fill \downarrow w/ \uparrow lat	Ambiguous	Ambiguous	F \downarrow w/ \uparrow lat

Table 3: Model-derived Values of Valley Shape as a Function of Depth

Depth D (m)	V-shape			U-shape			
	Top Width W_T (m)	Width-to-depth ratio F_V	Wall Angle θ	Top Width W_T (m)	Bottom Width W_B (m)	Wall Angle, θ	Width-to-depth ratio F_U
50	1378.8	27.6	4.2°	2145.6	896.2	4.6°	42.9
100	1935.8	19.4	5.9°	3084.6	1281.7	6.3°	30.9
150	2078.5	13.9	8.2°	3089.5	1181.0	8.9°	20.6
200	2251.6	11.3	10.1°	3752.5	1272.2	9.2°	18.8

Table 4: Extrapolation of U-shape Valleys via Filling to Original V-shape

Depth D (m)	Original Depth D_{orig} (m)	Fill Depth D_{fill} (m)	Original width-to-depth ratio F_{orig}	V-shape width-to-depth F_V
50	85.9	35.9	25.0	~21.7
100	171.1	71.1	18.0	~12.8
150	242.7	92.7	12.7	~9.9
200	302.5	102.5	12.4	~8.6

Table 5: Extrapolation of U-shape Valleys via Widening to Original V-shape

Depth D (m)	Original Top Width W_{Torig} (m)	Original width-to-depth ratio F_{orig}	V-shape width-to-depth F_V
50	1242.9	24.9	27.6
100	1811.6	18.1	19.4
150	1915.7	12.8	13.9
200	2469.7	12.3	11.3

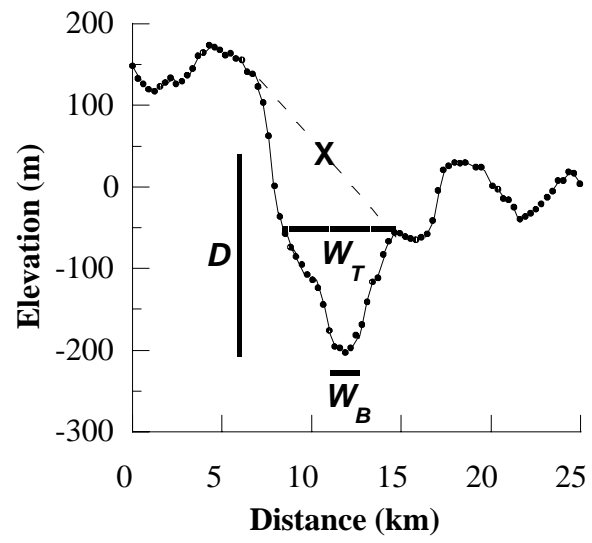


Figure 1

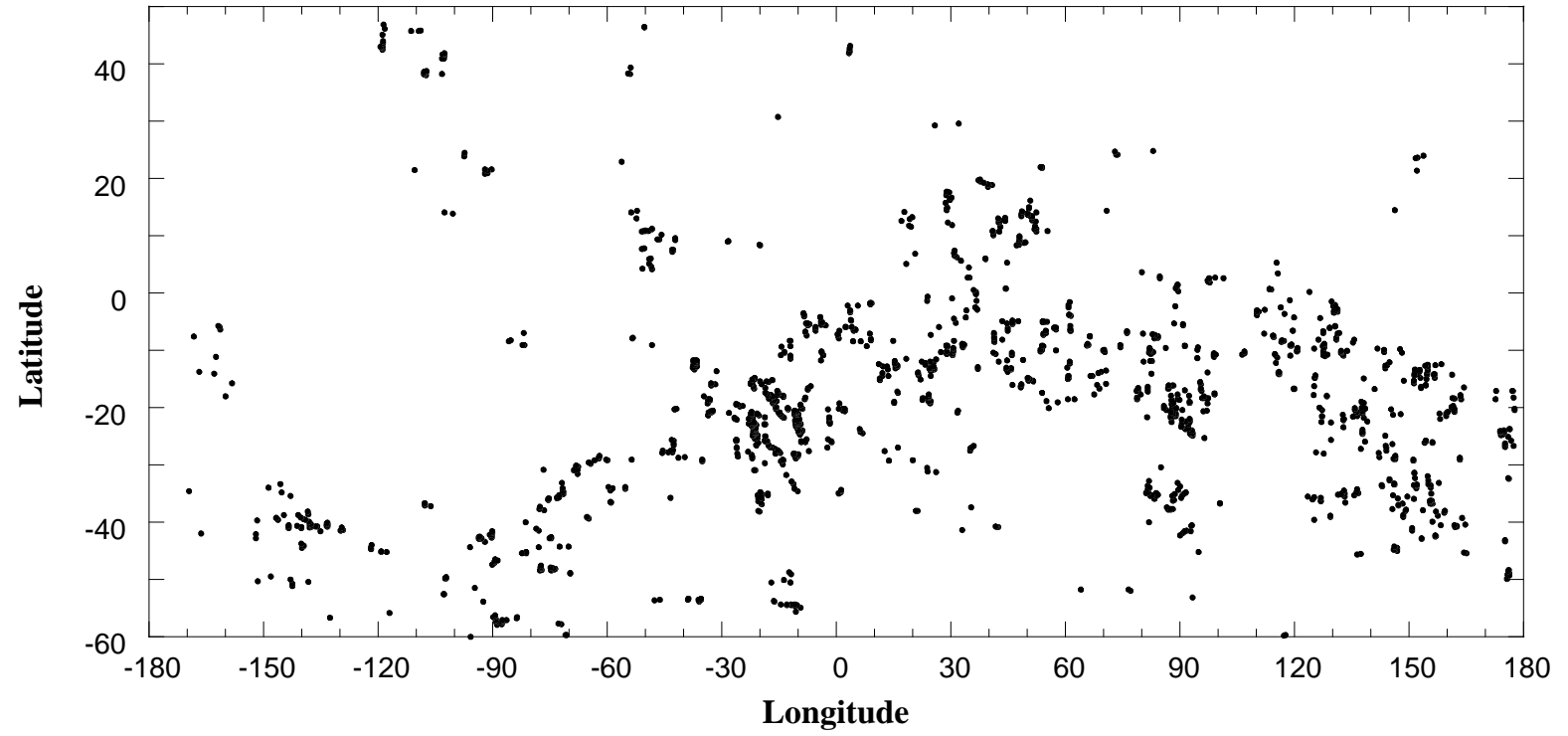


Figure 2

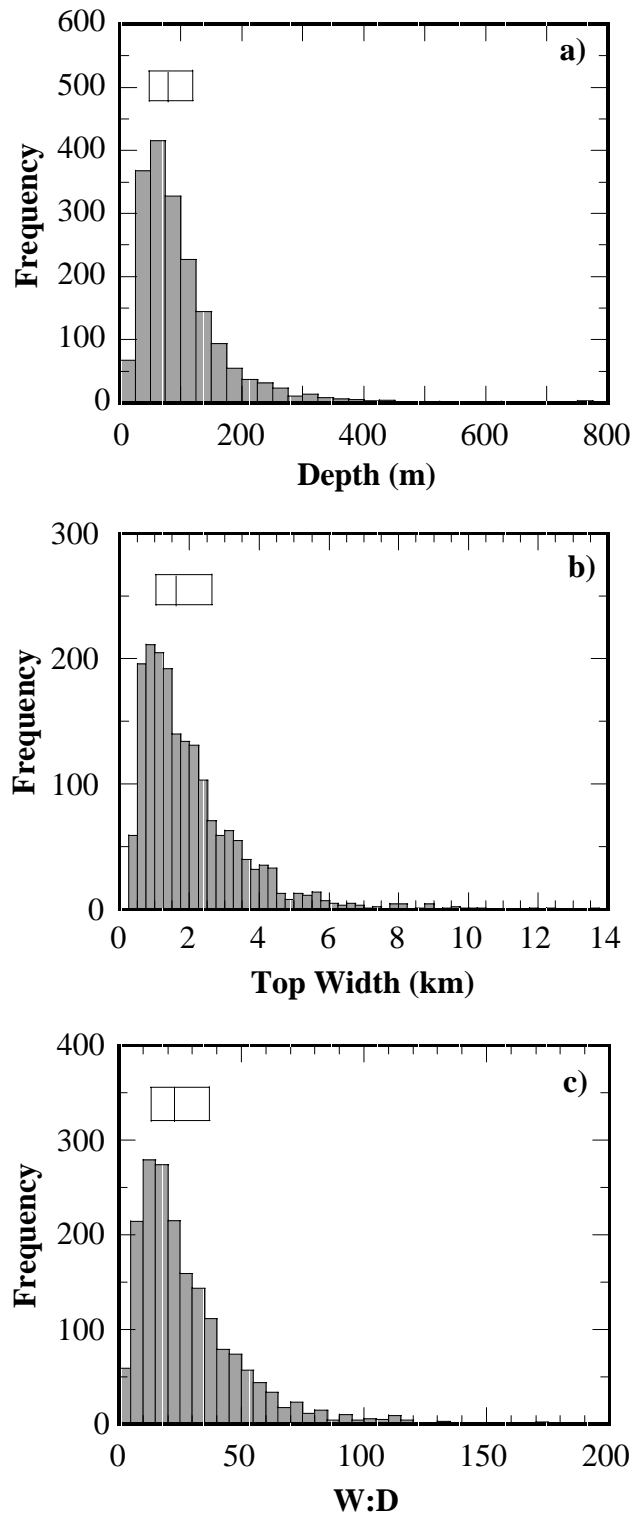


Figure 3

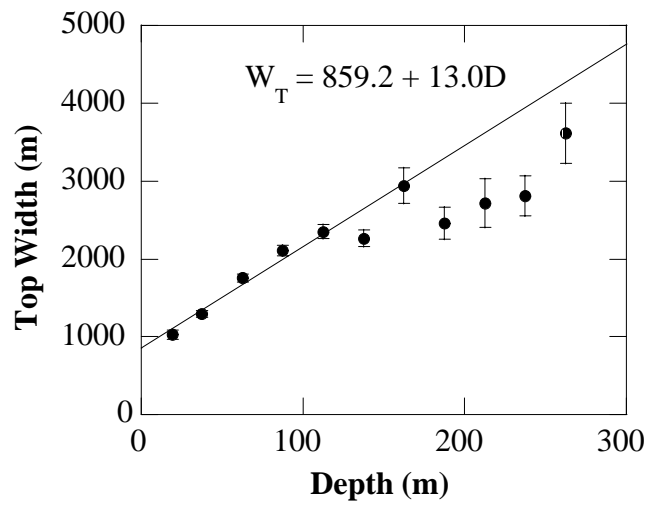


Figure 4

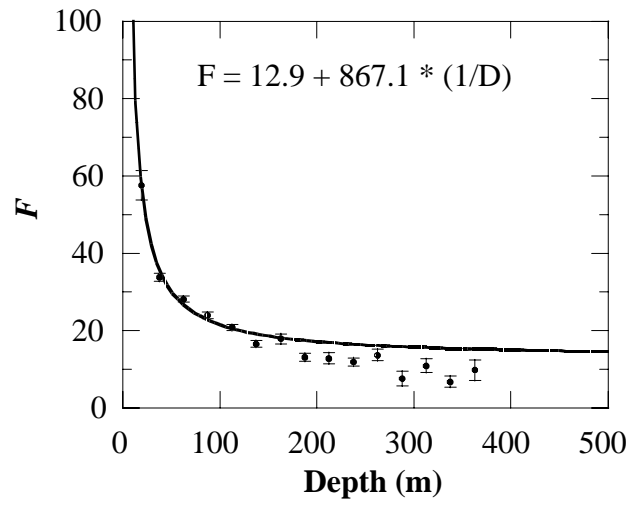


Figure 5

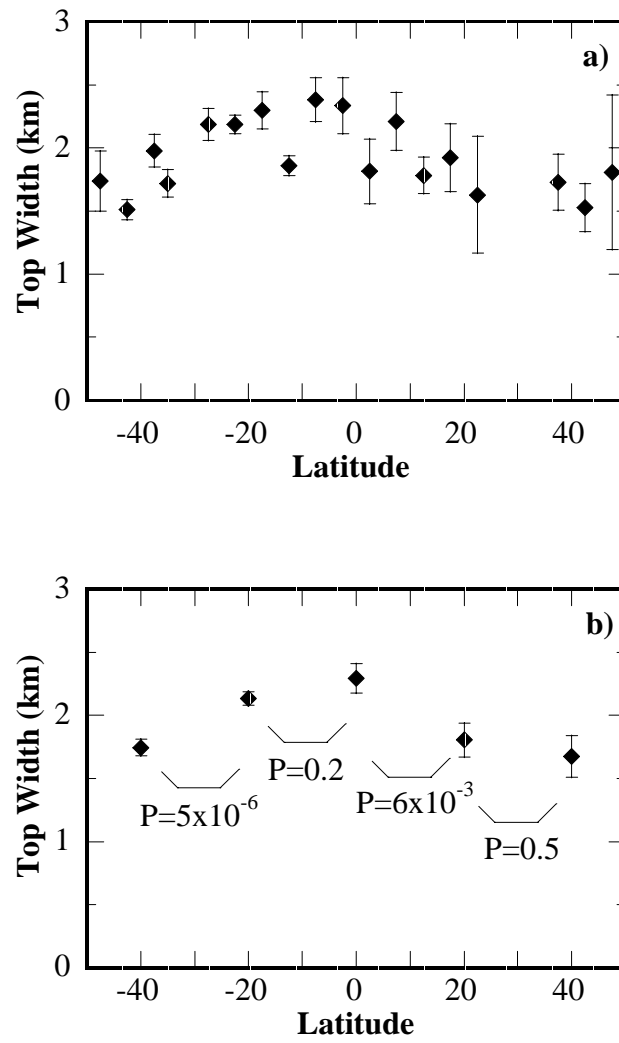


Figure 6

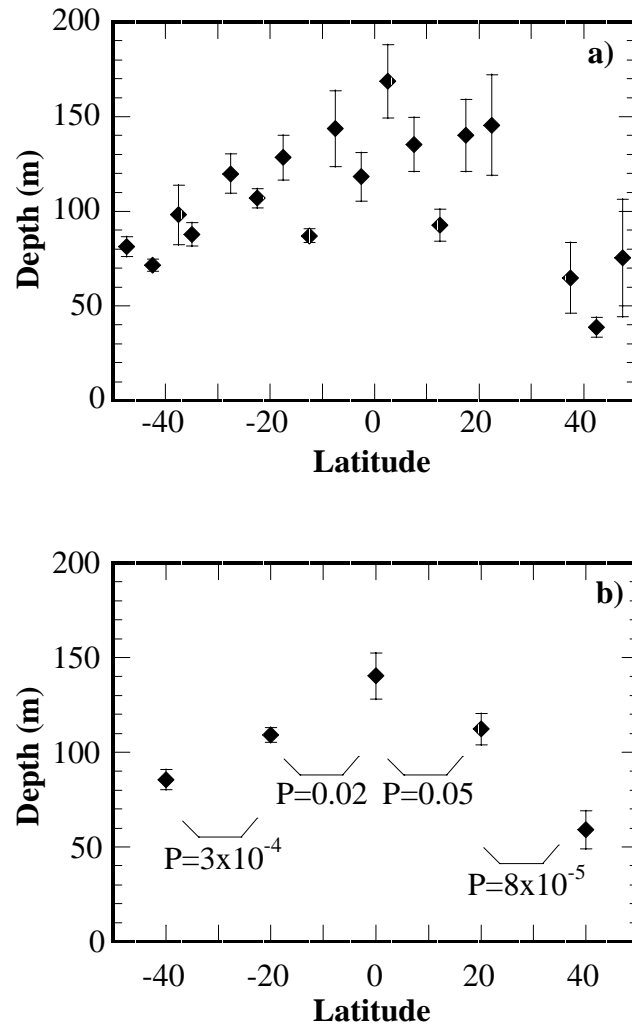


Figure 7

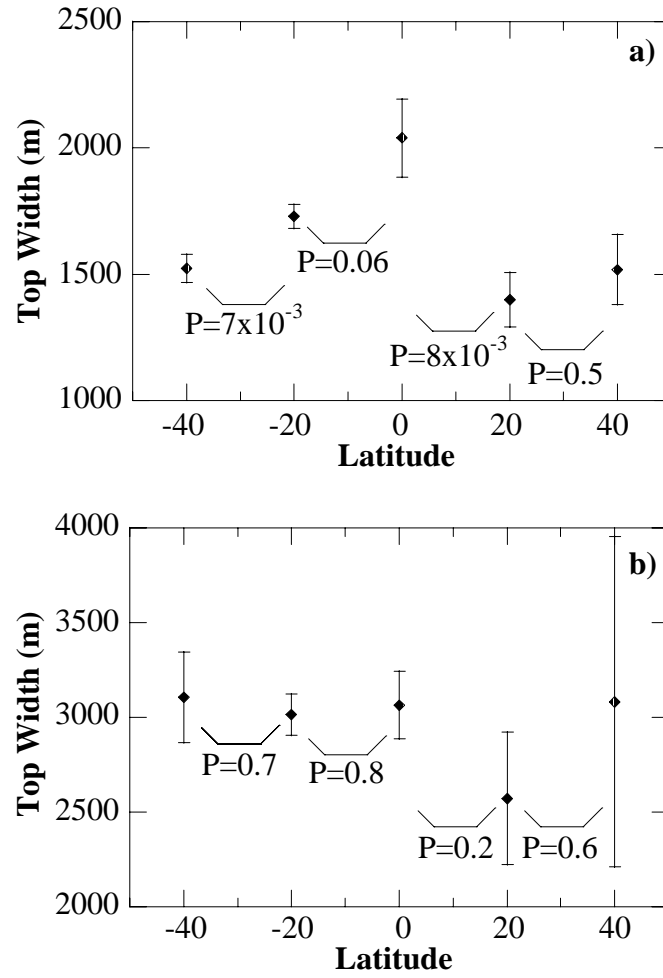


Figure 8

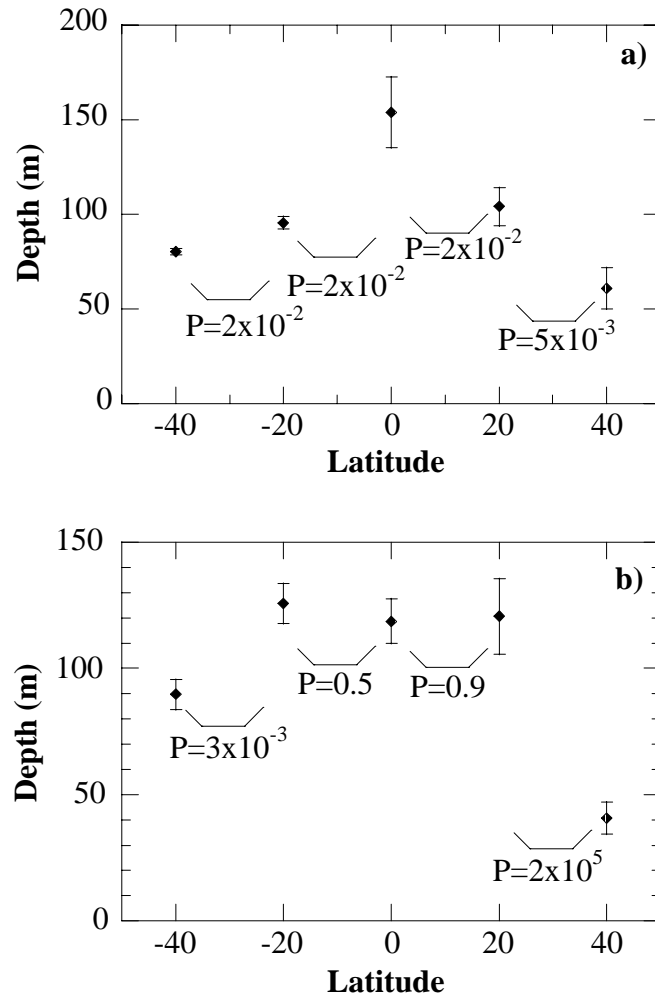


Figure 9

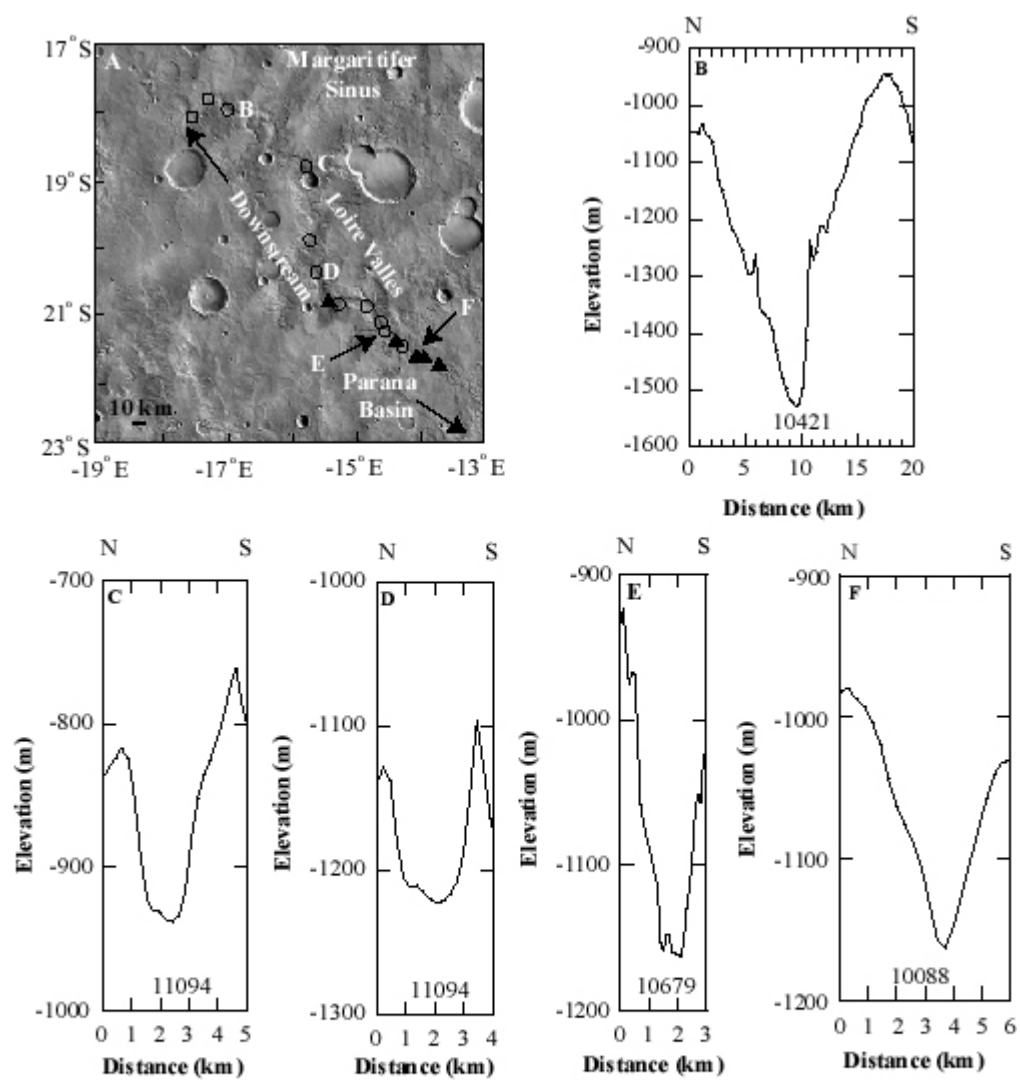


Figure 10

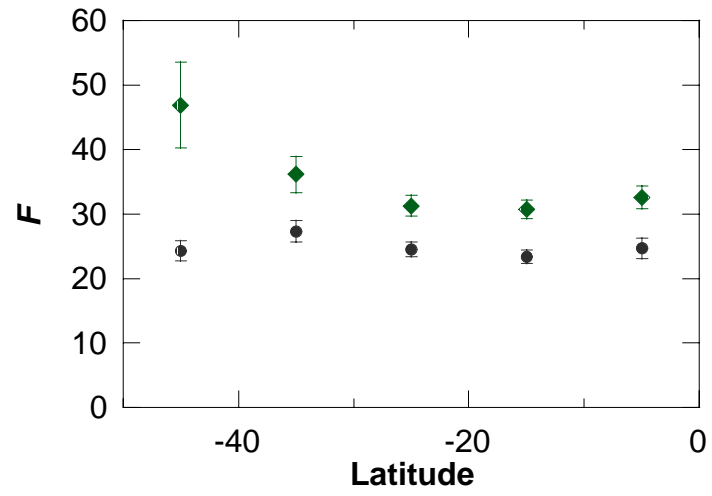


Figure 11

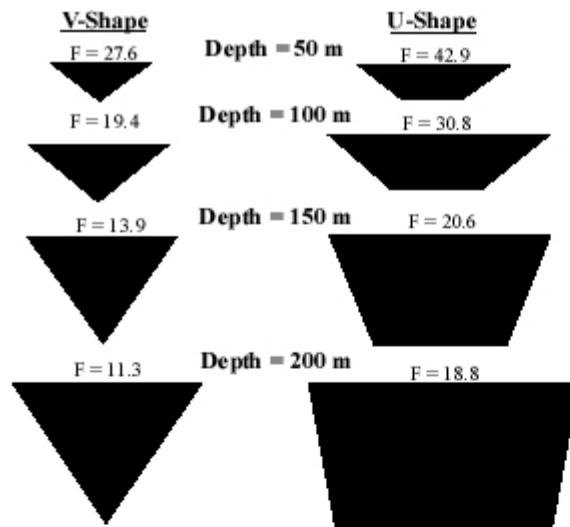


Figure 12

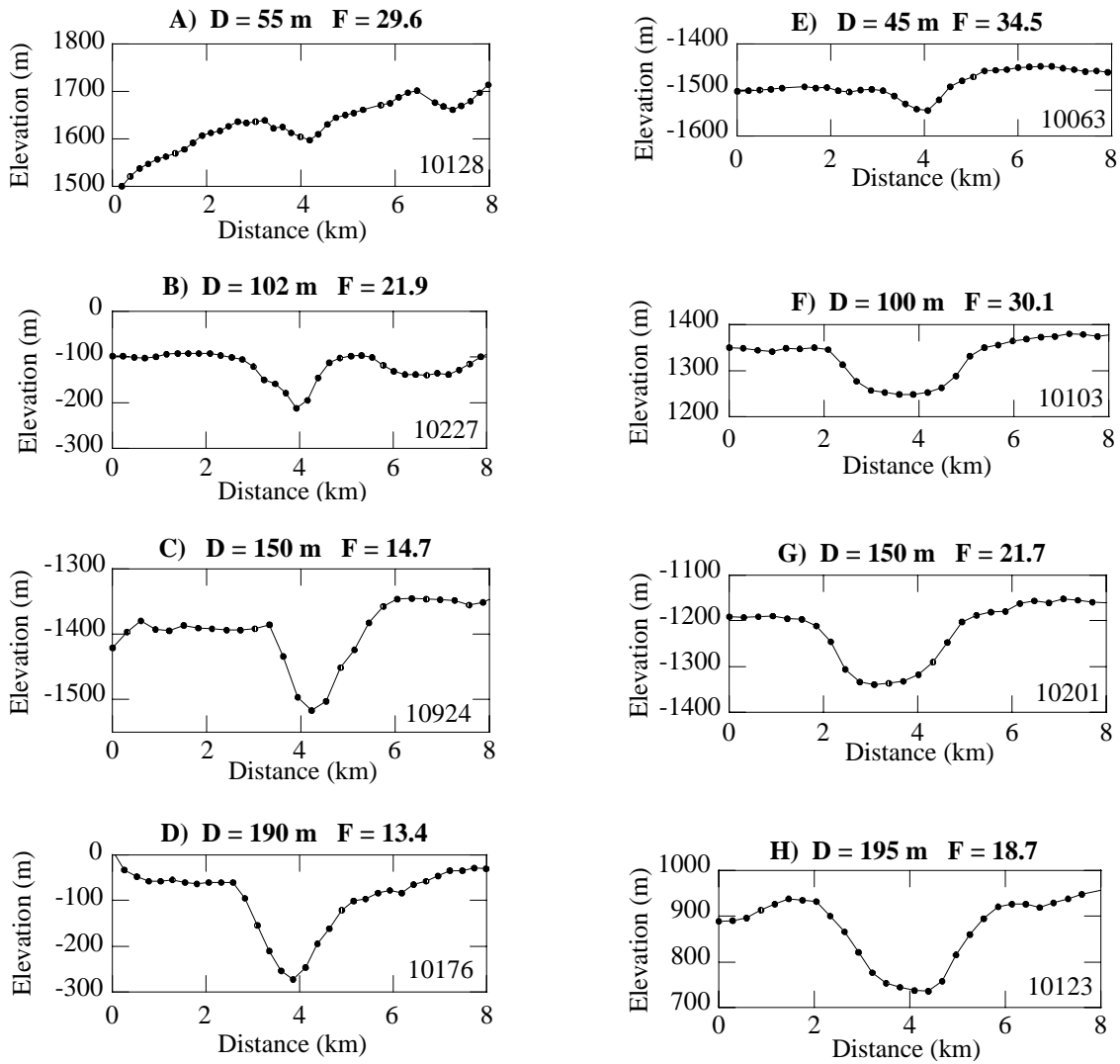


Figure 13

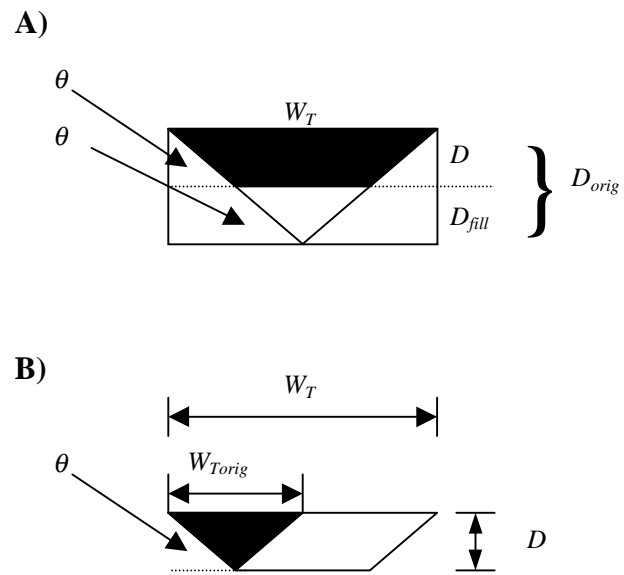


Figure 14